Macromolecular Materials and Engineering
Open Access
www.mame-journal.de

Wet Milling of Alginate Alco- and Hydrogel Composites: A Facile Top-Down Approach for Continuous Production of Aerogel Microparticles

Baldur Schroeter, Parnpailin Jeansathawong, Anja Hajnal, and Pavel Gurikov**

Moving toward high-throughput production of biopolymer aerogel microparticles, in this work, the wet milling process is applied to hydrogels and alcogels. Alcogels are then converted into aerogels by well-established supercritical drying. Alginate and hybrid alginate/silica gels are used as a model system. As the Young's moduli of hydrogels significantly change when water is exchanged by ethanol, it is possible to study the effect of the gel stiffness on macroscopic and microstructural properties of the resulting aerogels. Influence of process parameters (milling speed and gap size) is also investigated. Smallest particles sizes and minimal changes in microstructure are obtained for completely solvent exchanged gels. The wet milling is shown to be a versatile method to obtain aerogel particles with diameters in the range 50–300 µm.

1. Introduction

Aerogels are low-density and highly porous solid materials with high internal surface area, which were described for the first time by S. Kistler in 1931.[1] Since then, aerogels have been prepared from numerous materials, including silica, synthetic, biobased polymers, carbons, and metal oxides.[2] As a green and affordable alternative to synthetic polymers, biopolymer aerogels have shifted the focus of research in the last two decades.[3,4] The transfer to industrial production of biopolymer aerogels has still to be realized, though, and poses a challenge in the field.[5]

B. Schroeter, P. Jeansathawong
Institute for Thermal Separation Processes
Hamburg University of Technology
Eißendorfer Straße 38, 21073 Hamburg, Germany
E-mail: baldur.schroeter@tuhh.de
A. Hajnal, P. Gurikov
Laboratory for Development and Modelling of Novel Nanoporous Materials
Hamburg University of Technology
Eißendorfer Straße 38, 21073 Hamburg, Germany
E-mail: pavel.gurikov@tuhh.de

The ORCID identification number(s) for the author(s) of this article can be found under https://doi.org/10.1002/mame.202200674

DOI: 10.1002/mame.202200674

The production process of biopolymer aerogels generally involves: (1) gelation of a dissolved biopolymer followed by the formation of a hydrogel, (2) a solvent exchange (wherein water in the pores is replaced with another solvent), and (3) drying with supercritical carbon dioxide. The fabrication of biopolymer aerogels in particulate form has certain advantages:[6] the processing time (and presumably costs) of both solvent exchange and supercritical drying steps can be significantly reduced; furthermore, hydraulic conveying and other techniques from particle technology can be employed for handling of gel particles and dried aerogels. On the other hand, additional steps such as droplet generation and particle recovery are necessary. Different methods (e.g., conventional dropping method, vibration nozzle and electrostatic methods, and spraying approaches) are available for droplet generation from biopolymer solutions. The suitability of each approach depends on the physical properties of the employed fluids, gelation kinetics, and targeted particle properties, which influence, in particular, the particle size and sphericity.[6,7] Lately, the jet-cutting method, which is based on the mechanical cutting of a liquid jet, has gained attention as a versatile high-throughput method for the production of spherical biopolymer hydro- and aerogel particles in the size range of particle diameters $d_{particle}$ = 0.2–1.0 mm.[8–12] Limitations of the mentioned methods arise, i.a. from 1) the viscosity of applied biopolymer solution; 2) achievable particle sizes. Especially the continuous production of biopolymer microparticles in the range of $d_{particle} \leq 200$ nm still poses challenges at a larger scale. Another approach is the formation of spherical liquid biopolymer droplets in an immiscible oil phase, followed by gelation.[6] The benefits of so-called emulsion gelation methods are rooted in the high sphericity of obtained microparticles, and the relative simplicity in adjusting the particle size via variation of stirring parameters, oil-to-sol ratio, and surfactant concentration.[13] First studies showed the applicability of continuous operation mode at semi-industrial level.[14,15] Difficult separation of particles from the oil phase, costly and time-consuming washing steps, and need for additives (e.g., stabilizers and emulsifiers) are known drawbacks of the emulsion gelation technique.

An alternative approach to obtain micrometer-sized particles while avoiding these disadvantages is the use of top-down methods, in particular, down-milling of larger structures (e.g., millimeter-sized particles or larger monoliths). Principally,

milling of gels is feasible at any step of the aerogel production: in dry aerogel- as well as wet alco- and hydrogel state. Since the application of friction and shearing forces on carbon- and silica gels results in relatively easy breakup due to their brittle and stiff nature, milling in dry aerogel state may be a preferred approach for these material classes: grinding of carbon and silica aerogels has been carried out via manual mortar grinding, ultrasonic-, shaking-, and ball-milling processes,[16–18] among others. Depending on the milling process and applied forces, changes of the microstructure can occur, which depend on the amount of introduced energy.[17] Dry milling is, however, considered less suited for biopolymer-aerogels since they exhibit mechanical properties very different from inorganic aerogels, such as a certain degree of flexibility and plasticity, which is rooted in their fibrillar, foam-like microstructure.[19] Wet milling of suspended hydro- and alcogel biopolymer beads may be considered as an alternative due to the different viscoelastic properties of wet and dry gels. During wet milling, suspended materials are downsized by the shear forces provided by collisions of material beads with walls of the milling chamber, and the materials themselves.[20] Wet milling is established as a large-scale process, and mainly applied in food industry, e.g., for downsizing of corn and cereals.[20–22] In aerogel production, wet milling of solvent exchanged alcogels (pores filled with ethanol, EtOH) has recently been employed for the synthesis of hydrophobic silica aerogel microparticles using a colloid mill.[23] Factors affecting size reduction during colloidal wet milling can be classified into two main categories: factors related to the nature of raw materials and factors related to operating conditions. Rigidity, brittleness, and flexibility are examples of factors related to the material side, whereas milling speed, size of milling gap, and milling time can be adjusted from the processing side.[20,24] Mechanical properties of wet biopolymer gels are strongly dependent on the type of solvent/solvent mixture in the pores: for example, the solvent exchange from water to EtOH of initially elastic whey protein isolate hydrogels resulted in rigid alcogels, reflected in an increase of the Young's modulus E of the gels by a factor of 30.[25]

In this work, we aim to evaluate the potential of the wet milling process when applied to hydro- and alcogels in a colloid mill, which may allow to achieve a high-throughput production of biopolymer gel microparticles. Alginate gels are used in this work as a model system. Influence of the process settings (milling speed and gap size) on macroscopic and microstructural properties of the particles are investigated, as well as the effect of the Young's modulus of the initial gel. To assess capability of alginate to act as a binding matrix, colloidal silica was added to alginate as a filler material. The effect of the Young's modulus of wet gels was assessed by milling at different steps of the solvent exchange.

2. Experimental Section

2.1. Preparation of Alginate and Alginate-Silica Wet Gels

Sodium alginate powder (Hydagen 500, BASF) was added to demineralized water and stirred with an anchor stirrer at 600 rpm at room temperature for 4 h to achieve 2 L of a homogenous solution. For production of alginate-silica hybrid gels, colloidal silica solution (LUDOX AS-40) was added to aqueous sodium alginate at different weight ratios. The mixture was stirred at 600 rpm for another 2 h to achieve homogenous alginate/silica solutions. A small amount (<0.25 wt% with respect to the total solid mass) of pink pigment (Kremer Pigmente GmbH & Co. KG, Aichstetten, Germany) was added to enhance the contrast in image analysis. Alginate mass fraction in the sol of 2.0 wt% was kept constant throughout all experiments. Mass fraction of silica was varied, resulting in different overall content of alginate r_{alg} with respect to silica [wt%], from 10 to 100 wt%. A solution of 10 wt% calcium chloride dihydrate (Carl Roth, ≥99%) in demineralized water was used as gelation bath. Hydro- and alcogels were prepared in two different shapes: as cylindrical monoliths for mechanical testing and as particles for further downgrinding. Hydrogel monoliths were produced by transferring approx. 20 mL of the mixture into dialysis tubes (SERVAPOR, Serva, MWCO 12000–14000 RC, flat width 16 mm), which were sealed and immersed into 5 L of gelation solution for 3 days (Figure S1a, Supporting Information). Obtained hydrogels were cut to cylinders with heights between 10 and 14 mm and immersed in EtOH/water mixtures (EtOH 99.8% Carl Roth GmbH & Co. KG) with progressively increasing concentrations of ethanol for stepwise solvent exchange (Figure S1b, Supporting Information). The hydrogels were first subjected to an aqueous solution containing 25.0 wt% EtOH for 10 h. Then the EtOH concentration was increased to 50.0, 75.0, and 99.8 wt% for the same time until an EtOH concentration ≥99.0 wt% (determined by the density measurement, Anton Paar, DMA4500 M) was reached. For production of hydrogel beads, the jet-cutting method was applied following the process protocol in previous work[26] with following process settings: jet velocity = 1.89 m s^{-1}, nozzle diameter = 0.6 mm, number of wires in cutting disc = 24 with a diameter of 0.15 mm each, distance between nozzle and surface of gelation bath = 110 cm, cutting frequency = 2000 s^{-1}, nozzle inclination angle = 10°. So produced droplets were collected in 5.35 L of gelation solution for the formation of spherical hydrogel beads. Gelation solution was replaced after reaching a volume ratio 1:3 between the total volume of hydrogel beads and the volume of gelation solution. Hydrogel beads were separated from the gelation solution and submitted to the same solvent exchange protocol as described above for monoliths.

2.2. Wet Milling of Alginate and Alginate/Silica Beads

A colloid mill (IKA magic LAB) was used to reduce the particle size of wet gel beads produced via jet-cutting at different steps of the solvent exchange. The gap between rotor (Rotor MK, IKA magic LAB) and stator (Stator MK, IKA magic LAB) and the milling speed were varied. For each run, a volume of 100 mL wet beads was suspended in 2 L of demineralized water, EtOH/water mixture or 99.8 wt% EtOH, depending on the corresponding solvent exchange step. Milling speeds V_{mill} in the range of 10 000–26 000 rpm and mill gaps d_{gap} of 300, 600, and 900 µm were set, to cover a wide window of operating conditions. Suspended beads were fed into the mill and the resulting suspension of microparticles was collected in a bucket. Microparticles were allowed to settle down, and clear supernatant solution was poured off. Solvent exchange was completed for all particles by adding 99.8% EtOH. After an EtOH concentration ≥99.0 wt% was obtained, microparticles were sealed into filter paper bags and transferred to supercritical drying.

2.3. Supercritical Drying

Sealed particles were transferred into a high-pressure autoclave with a volume of 3.9 L and dried with supercritical CO_2 at a temperature of 70 °C and pressure of 120 bar for 5 h. Continuous flow of CO_2 was set to 30 g min^{-1}. After complete drying, the pressure in the autoclave was decreased at a rate of 2 bar min^{-1}. The aerogel particles were collected and kept in a desiccator prior to analysis to avoid moisture absorption.

2.4. Determination of Young's Modulus

Force–distance graphs of monolith samples were obtained using a texture analyser (TA.XTplusC Texture Analyzer, Stable Microsystems). Cylindrical monoliths were placed under the rod of the analyser for the compression test. A camera (DJI Osmo Pocket) was set to record videos of the compression test for each sample (Figure S2, Supporting Information). These videos were used to convert the force–distance curves to the true stress–strain curves which were used to identify Young's modulus in a further step (Figure S2, Supporting Information). True stress was calculated by dividing the applied force by the actual cross-sectional area of the samples, which changes continuously during the compression test (Figure S3, Supporting Information). The diameter of monoliths over compression tests were evaluated using a Python script, which was also used to generate the true stress–strain curves and to calculate the Young's modulus (Figure S4, Supporting Information). All measurements were carried out in triplicate, using three individual samples. It should be noted that the absolute values of Young's modulus for particles before and after upon milling may be different from the measurements on cylinders. From a practical viewpoint, it is however more useful to establish correlations between E-moduli measured on macroscopic samples and the characteristics of milled particles.

2.5. Determination of Volumetric Yield

In the course of the solvent exchange the gel volume decreases from V_0 to a certain volume V. Volumes were calculated from the dimensions of the gels: both diameter and thickness of wet cylindrical monoliths were determined by using a vernier scale. The degree of shrinkage is commonly expressed as the volumetric yield via Equation (1):

$$Y_V = \frac{V}{V_0} \tag{1}$$

For as-prepared gels $Y_v = 1$. It may drop to 0.1–0.8 in the course of solvent exchange.[3] The height and diameter of cylindrical gels were determined as single measurements. A standard error of 3% for height and diameter was estimated based on the results of prior triple determinations.

2.6. Volume Fraction of the Polymer and Scaling Relationship

Because biopolymer aerogels are usually processed from diluted biopolymer solutions, it can be assumed that the density of these solutions is close to that of water. Therefore, the volume fraction ϕ of the polymer in the as-prepared gel (subscript "0") can be calculated as follows:

$$\phi_0 = \frac{w}{100\rho_{sk}} \tag{2}$$

where ρ_{sk} is the polymer skeletal density (g cm^{-3}) and w is mass of the biopolymer (in g) in 100 g of the solution (which occupies ≈100 cm^3). The polymer volume fraction in a shrunk gel with Y_v is

$$\phi = \frac{w}{100 Y_v \rho_{sk}} \tag{3}$$

and thus, the relative change in the volume fraction in the solvent exchange is given as

$$\frac{\phi}{\phi_0} = \frac{1}{Y_v} \tag{4}$$

In the spirit of theoretical considerations by Sakai,[27] the normalized Young's modulus (E/E_0) of a partially shrunk (or swollen) gel scales with ϕ as:

$$\frac{E}{E_0} = \left(\frac{\phi}{\phi_0}\right)^m \tag{5}$$

where E_0 is the Young's modulus of the as-prepared gel and m is the scaling exponent. Combining Equations (4) and (5), this work finally arrived at the scaling relation used in this work:

$$\frac{E}{E_0} = Y_v^{-m} \tag{6}$$

Equation (5) provides a link between shrinkage and mechanical properties of polymer gels. As demonstrated by Sakai,[27] the exponent m takes different numerical values in dilute and semidilute regions. In this work, for the first time, the applicability of Equation (6) was tested for the processing of biopolymer aerogels.

For the estimation of the initial volume fraction, Equation (2), the skeletal density of calcium cross-linked alginate ($\rho_{sk,\,alg} = 1.89 \pm 0.13$ g cm^{-3}) was calculated from literature data (**Table 1**). The skeletal density of composite alginate-silica gels was estimated from the corresponding values of pure components:[28]

$$\rho_{sk} = \frac{1+r}{\frac{1}{\rho_{sk,\,alg}} + \frac{r}{\rho_{sk,\,sil}}} \tag{7}$$

A value of 2.2 g cm^{-3} was taken for the skeletal density of silica, $\rho_{sk,\,sil}$.[29]

2.7. Specific Surface Area and Pore Size Distribution

In case of monoliths, representative pieces were cut out for gas sorption analysis, microparticles were used directly. A total sample mass of approx. 20 mg was used for each run. All samples were degassed under vacuum at 60 °C for 4 h prior to low temperature N_2 adsorption–desorption analysis (Nova 3000e Surface Area Analyzer, Quantachrome Instruments, Boynton

Table 1. Skeletal density of calcium cross-linked alginate aerogels.

Mass fraction of alginate in initial solution [wt%]	Skeletal density [g cm^{-3}]	Reference
1.0	2.02 ± 0.08	[30]
1.0	1.92 ± 0.03	[30]
1.5	1.82	[31]
2.0	2.07 ± 0.02	[30]
2.0	1.934 ± 0.006	[30]
2.0	1.97 ± 0.03	[32]
2.0	1.95 ± 0.02	[32]
3.0	1.89 ± 0.02	[33]
3.0	1.85	[31]
5.0	0.366	[34]
5.0	1.77	[31]
6.0	1.18 ± 0.16	[35]
10.0	1.84	[31]
Median value ± IQR[a)]	1.89 ± 0.13	

[a)] Due to certain scattering of the literature data, the median was calculated as a measure of central tendency and the interquartile range (IQR) is a measure of statistical dispersion.

Beach, USA). Specific surface area S_V was determined using the Brunauer–Emmett–Teller (BET) method. The pore volume and mean pore diameter were estimated via Barrett–Joyner–Halendia (BJH) method.

2.8. Image Analysis of Hydrogel and Alcogel Beads Produced via Jet-Cutting

The size and shape of wet particles were assessed by evaluating images captured with an optical microscope (VisiScope TL384H, VWR International GmbH Darmstadt) via image analysis (Software ImageJ), the mean particle diameter (d_{mean}) was determined by evaluating at least 50 particles for each experiment. The mean particle diameter was calculated by taking the average of the largest and lowest diameters. The mean particle diameter of aerogels microparticles $d_{particle}$ and sphericity SPH of dry aerogel particles were determined via Camsizer XT system (Retsch Technology) according to previous work.[11]

3. Results and Discussion

3.1. Mechanical Properties and Shrinkage of Wet Gels

Mechanical properties and shrinkage of pure alginate and alginate-silica hybrid gels were monitored over different steps of the solvent exchange with EtOH. The volumetric yield Y_V of wet gels after solvent exchange has been reported to roughly correlate with the initial biopolymer content in the sol c_{biop} and to cover a wide range (Y_V = 5–95%). In addition, shrinkage depends heavily on solvent exchange strategies and individual properties of the gels, especially at low c_{biop}.[3] Summarized, a stepwise solvent exchange, high cross-linking degree, and high c_{biop} may help to mitigate shrinkage while replacing water with other solvents.[36] As for pure alginate gels in this work, a volumetric yield of approx. 85% was determined after complete solvent exchange (**Figure 1**a, red triangles). This value is comparatively high in comparison to already published data for alginate gels with low alginate content of c_{biop} = 0.5–3.0 wt% (Y_V = 20–60%), and may be attributed to the low EtOH gradient of approx. 20% used during solvent exchange and quantitative cross-linking of alginate due to the high concentration of Ca^{2+} in the gelation solution.[36] The sensitivity of pure alginate gels to solvent concentration varies over the steps of the solvent exchange, with no additional shrinkage occurring at ethanol concentrations $c_{EtOH} \geq 60\%$, which is in agreement with previous work showing that the effect of increasing gel stiffness can counterbalance further shrinkage at high c_{EtOH}.[3,36,37]

In contrast to pure alginate gels, change of Y_V of alginate-silica hybrid gels follows a strictly linear trend ($R^2 = 0.999$) (Figure 1a) over the entire course of the solvent exchange. The Young's modulus of different gels depends solely on ethanol concentration (Figure 1a) and addition of colloidal silica as filler material does not contribute to mechanical reinforcement.

As Equation (6) suggests, there should be a relation between the volumetric yield and the Young's modulus. Because the E_0 does not significantly depend on the gel composition (Figure 1a), Equation (6) is expected to hold true for all the gels. Indeed, all data points, expect a few outliers, fall on a master curve when the Young's modulus is plotted versus the volumetric yield (Figure 1b). To test the validity of the scaling relationship Equation (6), all Young's moduli determined in the course of the solvent exchange were normalized by the corresponding values of E_0 and plotted as a function of the volumetric yield in log–log coordinates (Figure 1c). Although the points do not collapse onto a single master curve, all curves have a similar shape and the slope at $Y_V = 1$, i.e., at the beginning of the solvent exchange. The numerical value of the slope ($m = 26.5 \pm 4.7$) is much larger than reported in the literature (0.33–1.1) for tetra-PEG swollen and shrunk gels in water and ionic liquids.[27] It is beyond the scope of this study to elucidate reasons for differences in the slope and effect of the gel nature on it. From a practical viewpoint, it is interesting to note that the scaling relation, Equation (6), may allow a broad classification of polymer gels with respect to the behavior in the solvent exchange process. Indeed, data for two other alginate gels (4 and 6 wt%, for production procedure see Supporting Information), which were not used in the milling, collapse roughly onto the same curve as all other alginate-containing gels (Figure 1c). When plotted on the same plot, literature data for protein gels[25] form a distinct family of curves (Figure 1c) with a much lower slope ($m = 3.7 \pm 1.3$).

The end point for all curves shown in Figure 1c is gel-specific and determined by Y_V and E at the end of the solvent exchange. In fact, the volumetric yield at the end of the solvent exchange can be estimated from the polymer weight fraction c_{pol} in the gel as follows (k_1 and k_2 are empirical parameters fitted to a large body of data):[3]

$$Y_V = 1 - (1 - k_1) \exp(-k_2 c_{pol}) \quad (8)$$

Therefore, measurements of the Young's modulus for pristine gel (E_0) and at the end of the solvent exchange are required to estimate the Young's modulus at any intermediate step of the solvent exchange. As we show in the following, the Young's modulus is

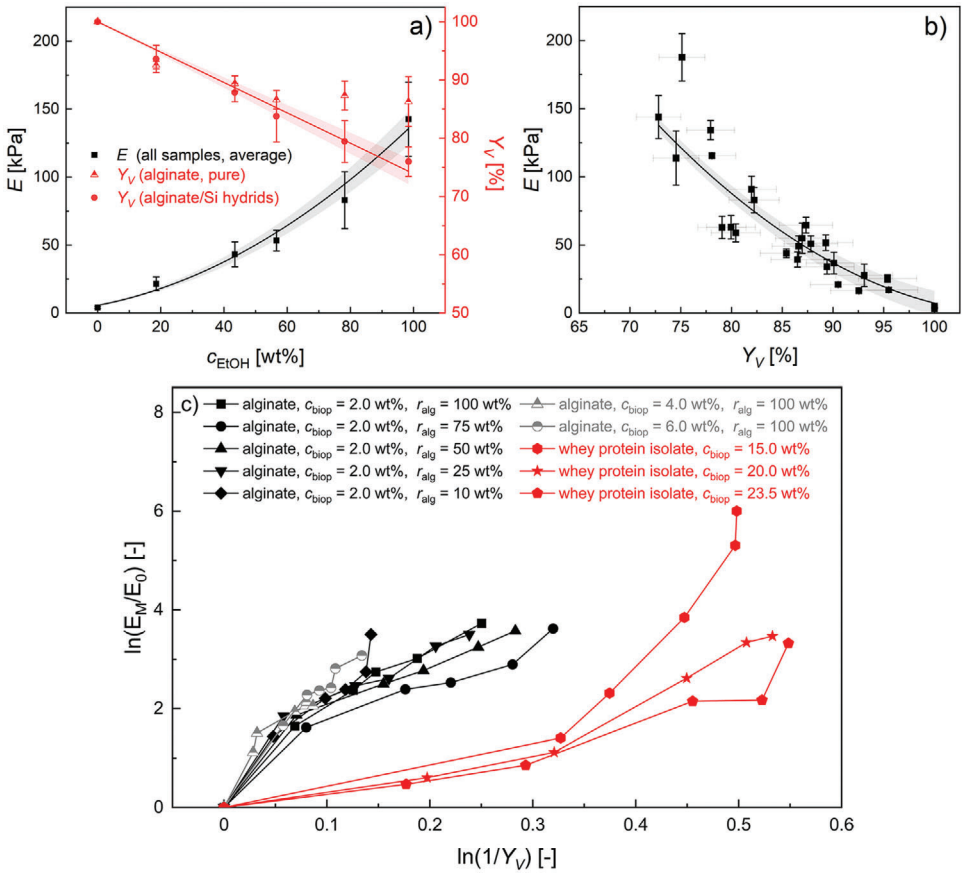

Figure 1. a) Change of volumetric yield (red) and Young's modulus (black) over the course of the solvent exchange. Red triangles represent data for pure alginate gels, error bars the standard deviation of the measurement. Red dots represent averaged data for alginate-silica hybrids with different silica amounts, errors bars represent the standard deviation ($n = 4$). Black squares represent change in the Young's modulus during solvent exchange, data is averaged for all gels, error bars represent the standard deviation ($n = 5$). Lines represent linear (red) and quadratic (black) fitting, areas the 95% confidence intervals. b) Relation between volumetric yield and Young's modulus of alginate-silica hybrid gels. The line represents quadratic fitting, area represents the 95% confidence interval. *y*-error is given as standard error of triple determinations ($n = 3$), *x*-error is given as standard error of the measurement. c) log–log representation of the scaling relation, Equation (6), between the Young's modulus and the volumetric yield in the course of the solvent exchange process. Besides 2 wt% alginate gel and silica-alginate hybrid gels, data for dense alginate gels (4 and 6 wt%) and protein gels are plotted.[25] Alginate-containing and protein gels form two distinct families with nearly the same slope at $Y_V = 1$, i.e., at the beginning of the solvent exchange.

a significant gel-specific parameter for the calculation of the particle size and particle sphericity after the wet milling. Hence, it is essential to be able to predict it from theoretical considerations. A detailed analysis of other types of gels with the scaling relation Equation (6) is a matter of our ongoing work.

3.2. Textural Properties

The influence of adding colloidal silica to the alginate matrix was compared at five different silica to alginate ratios (monolithic samples). A strictly linear relation ($R^2 = 0.997$, Figure S5a, Supporting Information) between S_V and r_{alg} was determined with lower S_V values at high silica content. This trend is attributed to the additional weight provided by the nonporous silica filler and shows that the filler material does not interfere with pore surfaces composed of calcium cross-linked alginate, nor contribute to the overall specific surface area by itself. Gas sorption results are in accordance with qualitative analysis of pore structure via SEM, whereas alginate pore network and colloidal silica particles are clearly identifiable as separated phases (Figure S5b, Supporting Information). The effect of wet milling on the microstructure was evaluated at maximum milling speed (V_{mill} = 22 000 rpm) and smallest gap size (d_{gap} = 300 µm) of the rotor stator system by passing dispersions of wet gel particles at different stages of the solvent exchange through the colloid mill at three different alginate to silica ratios. For all samples, no changes of specific surface area were detected after the milling process ($S_{V,\,average}$ = 517 m^2g^{-1} at r_{alg} = 100 wt%, $S_{V,\,average}$ = 342 ± 21 m^2g^{-1} at r_{alg} = 50 wt%, $S_{V,\,average}$ = 164 ± 9 m^2g^{-1} at r_{alg} = 10 wt%).

Fore pure alginate gels, changes in the microstructure occurred due to milling, whereas the ethanol content in the gels during milling ($c_{EtOH,\,mill}$) played a major role, as reflected by values of V_{meso}, and pore size distributions (**Figure 2**b). For hydrogels, significant increase of mesopore volume and narrowing of pore size distributions were observed after milling. This result is

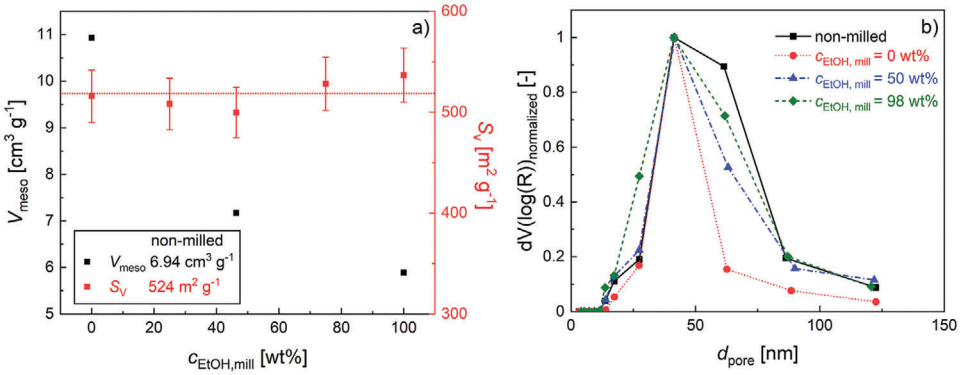

Figure 2. a) Specific surface area (red) and meso pore volume (black) of pure alginate aerogel microparticles obtained from wet-milling at fixed milling conditions (d_{gap} = 300 µm, V_{mill} = 22 000 rpm) and different steps of the solvent exchange in comparison to nonmilled particles. Dashed line corresponds to average S_V of all samples, error bars correspond to estimated standard error of Brunauer–Emmett–Teller (BET)/Barrett–Joyner–Halendia (BJH) methods. b) Normalized pore size distributions. Lines are drawn to guide the eye.

Table 2. Predicted range of model responses and significance of statistical models and model terms.

Model output	R^2_{model}	$R^2_{adj.}$	$R^2_{pred.}$	Significant model terms	Range
$d_{particle}$	0.905	0.901	0.896	E, d_{gap}, V_{mill}, r_{alg}	50.2–385.8 µm
SPH	0.800	0.792	0.781	E, r_{alg}	0.6–0.8

indicative for conversion of macropores and larger mesopores to smaller mesopores, e.g., by partial compression of the existing pore structure. Furthermore, the change of textural properties is less pronounced with increasing ethanol content in the gel, and only slight changes occur after the wet milling of completely solvent exchanged gels. It is interesting to note that this trend is in accordance with results reported by Schwan et al., who observed that the mesopore volume of ductile carbon aerogels increased after dry milling, while the mesopore volume of stiff carbon aerogels remained nearly unchanged.[17] In our case, we can conclude that stiffer and more rigid biopolymer fibers of alcogels are better able to withstand the friction forces in the wet milling process than the more flexible fibers of hydrogels, which are comparably easily deformed.

3.3. Size and Shape of Aerogel Microparticles

Wet-milling resulted in particles size distributions of various broadness: narrowest particle size distributions were obtained in all cases for complete solvent exchanged alcogels, whereas process parameters played a generally minor role (Figures S6–S8, Supporting Information). Regression analysis was used to determine significant influence factors (ANOVA: Tables S1 and S2, Supporting Information) affecting dry aerogel mean microparticle size and shape after the milling process. Results are based on 120 different settings (Table S3, Supporting Information) of different milling process parameters (V_{mill} and d_{gap}) and gels properties (E and r_{alg}).

Final particle size depends on all influence factors, whereas a broad range of $d_{particle}$ is accessible in the investigated range (**Table 2**). Relation of $d_{particle}$ follows linear process order in dependence of E, d_{gap}, V_{mill}, and quadratic process order in dependence of r_{alg} (Equation 9)

$$\sqrt{d_{particle}} = 13.51 - 5.46\,10^{-2} \times E + 3.66 \times 10^{-3} \times d_{gap} - 6.66 \times 10^{-5} \times d_{mill} + 0.15 \times r_{alg} - 1.09 \times 10^{-3} \times r_{alg}^2 \quad (9)$$

Sphericity of particles depends solely on properties of gels and is most adequately described by full quadratic process order (Equation 10)

$$\sqrt{SPH} = 0.78 + 1.50 \times 10^{-3} \times E + 8.64 \times 10^{-4} \times r_{alg} - 4.93 \times 10^{-6} \times E \times r_{alg} - 5.03 \times 10^{-6} \times E^2 - 9.99 \times 10^{-6} \times r_{alg}^2 \quad (10)$$

Lower particle sizes are generally achieved at high V_{mill}, low d_{gap}, and for complete solvent exchanged, stiffer gels (**Figure 3**a). Generally, gels properties have higher influence on particles size and shape as compared to process settings, with Young's modulus being by far the most significant influence factor. For instance, difference in final particle size after milling of pure alginate hydrogels as compared to completely solvent-exchanged alcogels is about 200 µm. Lowering the amount of alginate in composite gels results in slight additional reduction in the particles size (Figure 3b), showing, that introduction of colloidal silica into the alginate matrix creates addition breaking points and leads therefore to a more pronounced downgrinding of gels in the mill head.

This is also reflected by the trend of SPH: Breakup of nonsolvent exchanged gels and pure alginate gels results in irregular shaped gel shreds, more granular material with higher sphericity

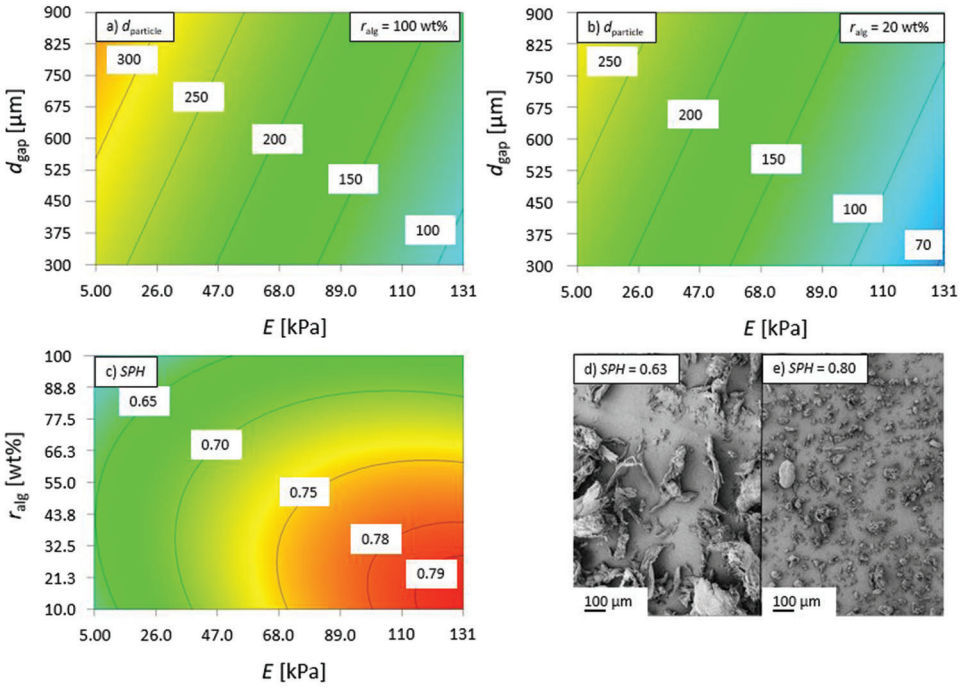

Figure 3. a–c) Contour plots: a) particle size d_{50} in dependence of E and d_{gap} at fixed r_{alg} = 100 wt% and V_{mill} = 26 000 rpm, b) particle size in dependence of E and d_{gap} at fixed r_{alg} = 20 wt% and V_{mill} = 26 000 rpm, c) sphericity in dependence of E and r_{alg}. d–e) Exemplary SEM pictures of aerogel particles derived from wet milling: d) r_{alg} = 20 wt%, $c_{EtOH,\ mill}$ = 0 wt%, d_{gap} = 300 µm, V_{mill} = 22 000 rpm, e) r_{alg} = 20 wt%, $c_{EtOH,\ mill}$ ≥99 wt%, d_{gap} = 300 µm, V_{mill} = 22 000 rpm.

is obtained by milling of solvent exchanged gel (Figure 3c–e). A qualitative assessment of the results to categorization via Krumbein/Sloss diagram is in agreement of particles shape in obtained range of SPH with low roundness (Figure S9, Supporting Information).[38]

While the quantitative relations in this section are specific for the investigated material system, the main results are principally transferable to other biopolymers: smaller and more spherical particles are obtained via wet milling of stiffer gels, which may, e.g., be achieved by maximizing biopolymer content and cross-linking degree in the gels as well as completing solvent exchange prior to milling.

4. Conclusions

On the way to high-throughput production of biopolymer aerogel microparticles, here we explored the wet milling process of hydrogels and alcogels, using alginate and hybrid alginate/silica gels as a model system. The gels were observed to lose their volume (shrinkage) and become stiffer (increase in the Young's modulus) in the course of the solvent exchange from water to ethanol. Alginate gels retained of ≈85% volume upon the solvent exchange and did not significantly shrink above 60 wt% EtOH. Hybrid alginate/silica gels, in contrast, shrink linearly with ethanol concentration. Changes in the Young's modulus of all studied gels were shown to depend solely on ethanol concentration, and not on the amount of silica (i.e., no reinforcement effect of silica was detected). A roughly universal relation was shown to exist between shrinkage and Young's moduli. When normalized by the Young's modulus of starting hydrogel and plotted in log–log coordinates, data for all studied gels form a family of curves, which are distinct from literature data on protein gels. Based on this observation, a new approach for the evaluation of Young's modulus at any intermediate step of the solvent exchange was suggested. The effect of wet milling on the microstructure of wet gel particles at different stages of the solvent exchange was evaluated. No changes in specific surface area were detected after the milling process for all gel compositions at all stages of the solvent exchange. A significant increase in mesopore volume and narrowing of pore size distributions were observed after milling of pristine hydrogels. These changes become less pronounced with increasing ethanol content in the gel, and only slight changes occurred after wet milling of fully solvent exchanged gels. Factors influencing size and shape of aerogel particles, which were produced from gels after the milling process, were elucidated with a multiple regression analysis. Gel-specific properties, mainly the Young's moduli, were found to be more important than parameters of the milling process for the estimation of both particles size and shape. Overall, wet-milling of hydro and alcogels offers a facile way for high throughput production of aerogel microparticles, whereas generally low sphericity (>0.8) represents the limiting factor for the use of the products, restricting the latter to applications which don't demand a round shape. For instance, high sphericity is a prerequisite for controlled release purposes or for further spray coating of aerogels beads.[39] Particles with low sphericity are desirable in all fields, which benefit from an entanglement of individual particles. Examples are the compression of aerogel particles to slabs, which represent from aerogel processing view an efficient way to build up larger aerogel structures, or 3D-printing of wet hydrogel particles.

Supporting Information

Supporting Information is available from the Wiley Online Library or from the author.

Acknowledgements

The manuscript was written through contributions of all authors. All authors had given approval to the final version of the manuscript. P.G. gratefully acknowledges support for this research from the German Research Foundation (DFG) under the project GU 1842/6-1.

Open access funding enabled and organized by Projekt DEAL.

Conflict of Interest

The authors declare no conflict of interest.

Data Availability Statement

The data that support the findings of this study are available from the corresponding author upon reasonable request.

Keywords

aerogel, alginate, colloid mill, microparticles, wet milling

Received: December 2, 2022
Revised: January 25, 2023
Published online:

[1] S. S. Kistler, *Cell Biol.* **1931**, *127*, 741.
[2] I. Smirnova, P. Gurikov, *Annu. Rev. Chem. Biomol. Eng.* **2017**, *8*, 307.
[3] P. Gurikov, R. P. Subrahmanyam, J. S. Griffin, S. A. Steiner, I. Smirnova, *Ind. Eng. Chem. Res.* **2019**, *58*, 18590.
[4] T. Budtova, D. A. Aguilera, S. Beluns, L. Berglund, C. Chartier, E. Espinosa, S. Gaidukovs, A. Klimek-Kopyra, A. Kmita, D. Lachowicz, F. Liebner, O. Platnieks, A. Rodríguez, L. K. Tinoco Navarro, F. Zou, S. J. Buwalda, *Polymers* **2020**, *12*, 2779.
[5] S. Zhao, W. J. Malfait, N. Guerrero-Alburquerque, M. M. Koebel, G. Nyström, *Angew. Chem.* **2018**, *130*, 7704.
[6] K. Ganesan, T. Budtova, L. Ratke, P. Gurikov, V. Baudron, I. Preibisch, P. Niemeyer, I. Smirnova, B. Milow, *Materials* **2018**, *11*, 2144.
[7] U. Prüsse, L. Bilancetti, M. Bučko, B. Bugarski, J. Bukowski, P. Gemeiner, D. Lewińska, V. Manojlovic, B. Massart, C. Nastruzzi, V. Nedovic, D. Poncelet, S. Siebenhaar, L. Tobler, A. Tosi, A. Vikartovská, K.-D. Vorlop, *Chem. Pap.* **2008**, *62*, 364.
[8] L. Druel, P. Niemeyer, B. Milow, T. Budtova, *Green Chem.* **2018**, *20*, 3993.
[9] U. Prüße, U. Jahnz, P. Wittlich, J. Breford, K. Vorlop, *Landbauforsch. Völkenrode, Sonderh.* **2002**, *241*, 1.
[10] I. Preibisch, P. Niemeyer, Y. Yusufoglu, P. Gurikov, B. Milow, I. Smirnova, *Materials* **2018**, *11*, 1287.
[11] B. Schroeter, V. P. Yonkova, N. A. M. Niemeyer, I. Jung, I. Preibisch, P. Gurikov, I. Smirnova, *Cellulose* **2021**, *28*, 223.
[12] C. López-Iglesias, J. Barros, I. Ardao, P. Gurikov, F. J. Monteiro, I. Smirnova, C. Alvarez-Lorenzo, C. A. García-González, *Polymers* **2020**, *12*, 273.
[13] R. S. Kumar, M. Vinjamur, M. Mukhopadhyay, *Int. J. Chem. Eng. Appl.* **2013**, *4*, 321.
[14] V. Baudron, P. Gurikov, I. Smirnova, S. Whitehouse, *Gels* **2019**, *5*, 12.
[15] N. V. Menshutina, D. D. Lovskaya, A. E. Lebedev, E. A. Lebedev, *Russ. J. Phys. Chem. B* **2017**, *11*, 1296.
[16] R. Reyhani, A. Zadhoush, N. S. Tabrizi, H. Nazockdast, M. Naeimirad, *J. Non-Cryst. Solids* **2021**, *571*, 121058.
[17] M. Schwan, J. Schettler, F. M. Badaczewski, C. Heinrich, B. M. Smarsly, B. Milow, *J. Mater. Sci.* **2020**, *55*, 5861.
[18] H. Yang, J. Wang, J. Zhang, P. Feng, Z. Wu, D. Yu, *J. Manuf. Process.* **2021**, *70*, 621.
[19] R. Chandrasekaran, M. Hillgärtner, K. Ganesan, B. Milow, M. Itskov, A. Rege, *Sci. Rep.* **2021**, *11*, 10198.
[20] W. Gao, F. Chen, X. Wang, Q. Meng, *Compr. Rev. Food Sci. Food Saf.* **2020**, *19*, 2222.
[21] M. Wronkowska, *J. Food Process. Preserv.* **2015**, *40*, 572.
[22] K. D. Rausch, D. Hummel, L. A. Johnson, J. B. May, *Corn Chemistry and Technology*, 3rd ed., AACC International Press, Washington, DC, USA **2019**.
[23] K. Zhang, T. Li, Z. Wang, Z. Sheng, X. Zhang, *J. Sol-Gel Sci. Technol.* **2022**.
[24] S. Sud, A. Kamath, *Int. Res. J. Pharm.* **2013**, *4*, 57.
[25] M. P. Dirauf, A. Hajnal, P. Gurikov, A. S. Braeuer, *Food Hydrocolloids* **2021**, *120*, 106916.
[26] S. Hofmann, C. Weiland, J. Fitschen, A. Von Kameke, M. Hoffmann, M. Schlüter, *Chem. Eng. J.* **2022**, *449*, 137549.
[27] T. Sakai, *Physics of Polymer Gels*, 1st ed., Wiley-VCH, Weinheim, Germany **2020**.
[28] P. Ratke, L. Gurikov, *The Chemistry and Physics of Aerogels: Synthesis, Processing, and Properties*, Cambridge University Press, NY, New York **2021**.
[29] L. T. Zhuravlev, *Colloids Surf., A* **2000**, *173*, 1.
[30] P. Paraskevopoulou, I. Smirnova, T. Athamneh, M. Papastergiou, D. Chriti, G. Mali, T. Čendak, G. Raptopoulos, P. Gurikov, *RSC Adv.* **2020**, *10*, 40843.
[31] I. Şahin, E. Uzunlar, C. Erkey, *J. Supercrit. Fluids* **2019**, *152*, 104571.
[32] G. Raptopoulos, I. Choinopoulos, F. Kontoes-Georgoudakis, P. Paraskevopoulou, *Polymers* **2022**, *14*, 1254.
[33] P. Paraskevopoulou, P. Gurikov, G. Raptopoulos, D. Chriti, M. Papastergiou, Z. Kypritidou, V. Skounakis, A. Argyraki, *Polyhedron* **2018**, *154*, 209.
[34] L. Baldino, S. Concilio, S. Cardea, E. Reverchon, *Polymers* **2016**, *8*, 106.
[35] A. Iglesias-Mejuto, C. A. García-González, *Mater. Sci. Eng., C* **2021**, *131*, 112525.
[36] R. Subrahmanyam, P. Gurikov, P. Dieringer, M. Sun, I. Smirnova, *Gels* **2015**, *1*, 291.
[37] A. Ghafar, P. Gurikov, R. Subrahmanyam, K. Parikka, M. Tenkanen, I. Smirnova, K. S. Mikkonen, *Composites, Part A* **2017**, *94*, 93.
[38] L. L. Krumbein, W. C. Sloss, *Stratigraphy and Sedimentation*, 2nd ed., W. H. Freeman and Co., San Francisco **1963**.
[39] B. Schroeter, V. P. Yonkova, M. Goslinska, M. Orth, S. Pietsch, P. Gurikov, I. Smirnova, S. Heinrich, *Cellulose* **2021**, *28*, 7795.